Journal of Power Sources 201 (2012) 18–25

Contents lists available at SciVerse ScienceDirect

Journal of Power Sources

journal homepage: www.elsevier.com/locate/jpowsour

Effects of (LaSr)(CoFeCu)$O_{3-\delta}$ cathodes on the characteristics of intermediate temperature solid oxide fuel cells

Sea-Fue Wang*, Chun-Ting Yeh, Yuh-Ruey Wang, Yung-Fu Hsu

Department of Materials and Mineral Resources Engineering, National Taipei University of Technology, 1, Sec. 3, Chung-Hsiao E. Rd., Taipei 106, Taiwan, ROC

ARTICLE INFO

Article history:
Received 9 September 2011
Received in revised form 17 October 2011
Accepted 19 October 2011
Available online 25 October 2011

Keywords:
Solid oxide fuel cell
Cathode
Microstructure
Impedance
Cell performance

ABSTRACT

In this study, Cu^{2+} ions doped $La_{0.6}Sr_{0.4}Co_{0.2}Fe_{0.8}O_{3-\delta}$ cathodes are prepared for use in solid oxide fuel cells (SOFCs). The maximum electrical conductivities of the $La_{0.6}Sr_{0.4}Co_{0.2}Fe_{0.7}Cu_{0.1}O_{3-\delta}$ (438 S cm^{-1}) and the $La_{0.6}Sr_{0.4}Co_{0.1}Fe_{0.8}Cu_{0.1}O_{3-\delta}$ (340 S cm^{-1}) discs are higher than that of the $La_{0.6}Sr_{0.4}Co_{0.2}Fe_{0.8}O_{3-\delta}$ disc (LSCF; 81 S cm^{-1}) sintered at 1100 °C. The substitution of Cu^{2+} over Fe^{3+} leads to a higher coefficients of thermal expansion (CTE), while the replacement of Co^{3+} by Cu^{2+} results in a lower CTE. Single cells with the $La_{0.6}Sr_{0.4}Co_{0.2}Fe_{0.8}O_{3-\delta}$, $La_{0.6}Sr_{0.4}Co_{0.2}Fe_{0.7}Cu_{0.1}O_{3-\delta}$, and $La_{0.6}Sr_{0.4}Co_{0.1}Fe_{0.8}Cu_{0.1}O_{3-\delta}$ cathodes operating at 650 °C and 550 °C show similar ohmic resistance (R_0) values while the polarization resistance (R_P) values of the cells with the $La_{0.6}Sr_{0.4}Co_{0.2}Fe_{0.7}Cu_{0.1}O_{3-\delta}$ and $a_{0.6}Sr_{0.4}Co_{0.1}Fe_{0.8}Cu_{0.1}O_{3-\delta}$ cathodes are slightly lower than that of the single cell with the $La_{0.6}Sr_{0.4}Co_{0.2}Fe_{0.8}O_{3-\delta}$ cathode, indicating that the Cu^{2+}-doped LSCF cathode exhibits a greater electrochemical catalytic activity for oxygen reduction. Maximum power densities of the cells with the $La_{0.6}Sr_{0.4}Co_{0.2}Fe_{0.8}O_{3-\delta}$, $La_{0.6}Sr_{0.4}Co_{0.2}Fe_{0.7}Cu_{0.1}O_{3-\delta}$, and $La_{0.6}Sr_{0.4}Co_{0.1}Fe_{0.8}Cu_{0.1}O_{3-\delta}$ cathodes operating at 700 °C read respectively 1.07, 1.15, and 1.24 W cm^{-2}. It is evident that the doping of Cu^{2+} ions in LSCF is beneficial to the electrochemical performance of the cells.

1. Introduction

Solid oxide fuel cell (SOFC) system has been attracting increased attention for commercialization because of its self-reforming ability, high energy conversion efficiency, no need of noble metals as catalysts, use of solid state materials, and compatibility with common hydrocarbon fuels [1,2]. Ideal for heat and power generation for homes and businesses, SOFCs can also be applied to large-size stationary power facilities as well as auxiliary power units for electrical systems in transportation vehicles. Able to operate at temperatures between 500 and 700 °C, intermediate temperature SOFCs (IT-SOFCs) in particular have become a popular R&D topic [3]. The performance of IT-SOFCs depends to a great extent on the ionic conductivity of the electrolyte and the polarization resistance (R_p) of the electrodes [4]. To improve the former feature, one may consider the replacement of electrolytes with higher ionic conductivity at low temperatures, such as $Sm_{0.2}Ce_{0.8}O_{2-\delta}$ (SDC) and $La_{0.9}Sr_{0.1}Ga_{0.8}Mg_{0.2}O_{3-\delta}$ (LSGM), or the use of a thin yttria-stabilized zirconia (YSZ) electrolyte film [5]. The cathode, on the other hand, is often the major source of the SOFC cell resistance because of its large overpotential, since oxygen reduction reaction is usually considered to be more exigent to activate on SOFCs operating at intermediate temperatures [6].

Thanks to their high electrical conductivities in an oxygen-containing atmosphere, several doped perovskite oxides, including $La_{1-x}Sr_xMnO_3$ (LSM), $La_{1-x}Sr_xFeO_3$ (LSF), $La_{1-x}Sr_xCoO_3$ (LSC), and $La_{1-x}Sr_xCo_{1-y}Fe_yO_3$ (LSCF), have been suggested to serve as the cathode materials for SOFCs. While $La_{1-x}Sr_xMnO_3$ (LSM) continues to be a top choice as the desired cathode material for use with YSZ at high temperatures (>850 °C), other cathodes have been recommended for use in IT-SOFCs whose performance tends to grow poorer at temperatures below 800 °C [6,7]. The performance of LSM cathode drops drastically as the operating temperature decreases, mainly due to its low oxygen ion conductivity and high activation energy for oxygen disassociation [6,8]. Hence, one strategy is to use materials with mixed ionic/electronic conductivity (MIEC) like $La_{0.6}Sr_{0.4}Co_{0.2}Fe_{0.8}O_{3-\delta}$ (LSCF), utilizing their high catalytic activity for oxygen exchange reaction and high electronic conductivity for current pickup to enhance the performance of the cathodes [9,10]. Single phase mixed conductors have been found to bring about dramatic improvement in the electrochemical performance of the cathodes since oxygen reduction can take place along the entire cathode–gas interface [8,11].

In our previous study [12], the effects of bi-layer cathodes, consisting of a current collector LSCF layer and a functional LSCF–SDC composite layer in various thicknesses, on the cell performance of SOFCs were reported. The results indicated that insertion of the composite layer is crucial for ensuring a good adhesion of the cathode layer to the electrolyte layer. However, the ohmic (R_0) and polarization resistances (R_P) escalated rapidly with the thickness

* Corresponding author. Tel.: +886 2 2771 2171x2735; fax: +886 2 2731 7185.
E-mail address: sfwang@ntut.edu.tw (S.-F. Wang).

0378-7753/$ – see front matter © 2011 Elsevier B.V. All rights reserved.
doi:10.1016/j.jpowsour.2011.10.074

of the LSCF–SDC composite layer in the cathode, especially at temperatures ≤550 °C. When the electrical and mechanical integrity of the single cell is taken into consideration, the composite layer should be kept as thin as possible so as to trim down the R_0 and R_P values and to prop up the cell performance. In this study, a different approach to improve the performance of cathodes in IT-SOFCs was explored by doping ions in the LSCF host materials. As reported in the literature, the conductivity and the polarization resistance of $La_{1-x}Sr_xCuO_{3-\delta}$ (LSCu) are significantly higher than those of LSM, though the coefficient of thermal expansion (CTE) of LSCu at $1.8 \times 10^{-6}\,K^{-1}$ to $17.9 \times 10^{-6}\,K^{-1}$ is much higher than that of YSZ ($\sim 10 \times 10^{-6}\,K^{-1}$) [13,11]. With Co^{2+} partially substituted by Cu^{2+} in $(La_{1-x}Sr_x)CoO_{3-\delta}$ (LSC), the ionic conductivity and the electrode activity of the $(La_{1-x}Sr_x)(Co_{1-y}Cu_y)O_{3-\delta}$ (LSCC) cathode appears to be better than those of its LSC counterpart, although the electrical conductivity of LSCC is lower [14]. Substituting Cu^{2+} for the $La_{1-x}Sr_xFeO_{3-\delta}$ (LSF) compound also results in a lower melting point and a higher power density [15,16]. Though Cu^{2+} substitution over B sites of the above perovskite oxides brings about a substantial improvement in the cathode performance at reduced temperatures [13,11,14–16], it has not been attempted in the LSCF cathodes. In this study, Cu^{2+} ions doped LSCF cathodes were used as potential cathode materials in order to enhance the electrode performance, since LSCF is a common cathode material for use with SDC electrolyte in IT-SOFC. The electrical conductivity and CTE of the prepared (La,Sr)(Co,Fe,Cu)$O_{3-\delta}$ (LSCFC) cathodes were determined first. IT-SOFCs were then built, using NiO–SDC, SDC, and LSCFC–SDC, respectively as the anode, electrolyte, and cathode, to facilitate the characterization and discussion of cell performance and impedance analysis.

2. Experimental procedure

2.1. Preparation of the cathode materials

The cathode powders used in this investigation were synthesized by solid state reaction method. Highly pure (>99.9% purity) La_2O_3 (SHOWA, Reagent grade), $SrCO_3$ (SHOWA, Reagent grade), Co_3O_4 (ALDRICH, Reagent grade), Fe_2O_3 (SHOWA, Reagent grade), and CuO (SHOWA, Reagent grade) were used as raw materials. Oxides based on the compositions of $La_{0.6}Sr_{0.4}Co_{0.2}Fe_{0.8}O_{3-\delta}$, $La_{0.6}Sr_{0.4}Co_{0.2}Fe_{0.7}Cu_{0.1}O_{3-\delta}$, and $La_{0.6}Sr_{0.4}Co_{0.1}Fe_{0.8}Cu_{0.1}O_{3-\delta}$ were mixed and milled in methyl alcohol solution using polyethylene jars and zirconia balls for 24 h and then oven dried at 80 °C for overnight. After drying, the powders were calcined at 950 °C for 4 h at a heating rate of 5 °C min^{-1}, and then re-milled in methyl alcohol for 24 h. Phase identification on the calcined powders was conducted using X-ray diffraction (XRD, Rigaku DMAX-2200) with Cu-Kα radiation (λ = 1.5418 Å). The scanning region 2θ was equal to 20–80° with step 0.05°. Jade 5 programs were adopted to analyze the experimental data. For measuring electrical conductivity, the powders were added with a 5 wt% of 15%-PVA solution and pressed into disc-shaped compacts under a uniaxial pressure of 0.9 tons cm^{-2}. The samples were then heat treated at 550 °C for 4 h to remove PVA, followed by sintering at 1100 °C to 1300 °C for 2 h (heating rate = 5 °C min^{-1}). Densities of the specimens were measured using the liquid displacement method. Scanning electron microscopy (SEM, Hitachi S4700) studies on the surfaces of the sintered discs were performed for microstructure examination. Conductivity as a function of temperature was measured by a standard four-probe method in air using Keithley 2400 in the temperature range of 25–800 °C. CTE (coefficient of thermal expansion) was determined from the dilatometer curve of the dense samples (NETZSCH 402C) at a heating rate of 5 °C min^{-1}.

2.2. Fabrication of single cells

Commercially available raw materials for SOFC, including $Sm_{0.2}Ce_{0.8}O_{2-\delta}$ (SDC; Fuel Cell Materials, USA; d_{50} = 0.53 μm and BET surface area = 6.2 $m^2\,g^{-1}$) and NiO (anode functional layer: Fuel Cell Materials, USA; current collector layer: SHOWA, Japan) were used in this study. Two kinds of NiO powders were used to fabricate the SOFCs. The one with a smaller particle size (d_{50} = 0.8 μm and BET surface area = 3.4 $m^2\,g^{-1}$) was used for anode functional layers to increase the TPB (triple-phase boundary) and, by extension, the electrochemical activity; the other with a larger particle size (d_{50} = 10.1 μm and BET surface area = 0.06 $m^2\,g^{-1}$) was used for the anode current collector layer to reduce the sintering shrinkage mismatch with other layers and to tailor the porosity of the layer. $La_{0.6}Sr_{0.4}Co_{0.2}Fe_{0.8}O_{3-\delta}$ (LSCF: Fuel Cell Materials, USA; d_{50} = 0.99 μm and BET surface area = 5.4 $m^2\,g^{-1}$) was also used as the cathode material for comparison.

The anode-supported substrates incorporate a SDC electrolyte layer and a three-layer anode composed of a current collector layer (outer layer) of pure NiO and two functional layers of NiO–SDC composites with ratios of 60 wt%/40 wt% and 50 wt%/50 wt%, respectively. The thin 50 wt% NiO/50 wt% SDC composite layer guarantees a good contact with the nearby electrolyte layer. The anode-supported substrates were fabricated using tape casting process with the dried and laminated tapes drilled into discs. The discs with a size of 25 mm in diameter and 0.5 mm in thickness were then co-fired at 1400 °C for 2 h at a heating rate of 2 °C min^{-1}. The cathode, prepared by screen-printing on the anode-supported SDC substrate, was fired at 1000 °C for 2 h. The porosity of the cathode layer was determined using mercury porosimetry (Micromeritics AUTOPORE 9520/NTUPT03).

2.3. Electrochemical characterizations

The electrochemical performance of the single cells was measured using a commercially available ProboStat (NorECs, Norway) system. Hydrogen humidified through water at room temperature was channeled into the anode side as fuel gas, and compressed air was delivered to the cathode side as oxidant gas. The flow rates of hydrogen and air were kept respectively at 40 and 160 sccm by electronic mass flow controllers. The pressures of hydrogen and air flows were controlled respectively at ≈1.04 bar and ≈1.10 bar by a pressure regulator with a graduated cylinder filled with water. The current density as a function of cell voltage (*I–V* curves) was measured under various applied loads across the cell, and evaluations were carried out from 500 to 700 °C at an interval of 50 °C. Electrochemical impedance spectra (EIS) were measured after holding the cells under OCV (open circuit voltage) for 15 min at the temperatures ranging from 500 to 700 °C. The EIS measurements were performed with a four-lead two-electrode configuration using a multi-channel potentiostat/galvanostat (Solartron 1470E) and a 1260 frequency response analyzer with a computer interface and Corr-view software. The frequency ranged from 10^5 Hz to 0.015 Hz, and the signal amplitude read 10 mV. *I–V* curves and power curves were obtained using linear sweep from OCV to 0.2 V at a sweep rate of 5 mV s^{-1}. After testing, the cross-section microstructure of the cells was examined by SEM.

3. Results and discussion

XRD results showed that pure perovskite phase could not be achieved when $La_{0.6}Sr_{0.4}Co_{0.2}Fe_{0.8}O_{3-\delta}$ was calcined at temperatures of 950 °C and lower; a second phase of CuO, however, was detected when the Cu^{2+} doped $La_{0.6}Sr_{0.4}Co_{0.2}Fe_{0.8}O_{3-\delta}$ was calcined at temperatures of 1150 °C and higher. The calcination

Table 1
Lattice parameters and physical properties of $La_{0.6}Sr_{0.4}Co_{0.2}Fe_{0.8}O_{3-\delta}$, $La_{0.6}Sr_{0.4}Co_{0.2}Fe_{0.7}Cu_{0.1}O_{3-\delta}$, and $La_{0.6}Sr_{0.4}Co_{0.1}Fe_{0.8}Cu_{0.1}O_{3-\delta}$ cathodes.

Cathode	Lattice constant		c/a	Theoretical density ($g\,cm^{-3}$)	TEC ($1\,K^{-1}$, 25–800 °C)	Maximum electrical conductivity ($S\,cm^{-1}$)
	a (Å)	c (Å)				
$La_{0.6}Sr_{0.4}Co_{0.2}Fe_{0.8}O_{3-\delta}$	5.4871	2.4298	2.4298	6.387	15.9×10^{-6}	81 (400 °C)
$La_{0.6}Sr_{0.4}Co_{0.2}Fe_{0.7}Cu_{0.1}O_{3-\delta}$	5.4544	2.4559	2.4559	6.456	17.6×10^{-6}	438 (400 °C)
$La_{0.6}Sr_{0.4}Co_{0.1}Fe_{0.8}Cu_{0.1}O_{3-\delta}$	5.4692	2.4421	2.4421	6.430	12.2×10^{-6}	340 (350 °C)

temperatures of 1000 °C and 1100 °C were therefore selected to synthesize the cathode materials. It was found that the Cu^{2+} content, when exceeding 30% of B-site ions, triggered the formation of the second phase of CuO. As revealed in Fig. 1 that shows the XRD patterns of the $La_{0.6}Sr_{0.4}Co_{0.2}Fe_{0.8}O_{3-\delta}$, $La_{0.6}Sr_{0.4}Co_{0.2}Fe_{0.7}Cu_{0.1}O_{3-\delta}$, and $La_{0.6}Sr_{0.4}Co_{0.1}Fe_{0.8}Cu_{0.1}O_{3-\delta}$ powders calcined at 1000 °C for 4 h and indexed using JCPDS 00-048-0124, a rhombohedrally distorted perovskite-like structure (space group $R\bar{3}c$) emerged after calcination. No visible second phase was observed in the XRD patterns. As indicated by the lattice parameters and c/a ratios of the samples listed in Table 1, lattice parameter a dropped while lattice parameter c rose with the Cu^{2+} ion substitution. The c/a ratio is generally used to characterize the Jahn–Teller distortion of the oxygen octahedron around the B-site ions [17]. The c/a ratios of $La_{0.6}Sr_{0.4}Co_{0.2}Fe_{0.7}Cu_{0.1}O_{3-\delta}$ and $La_{0.6}Sr_{0.4}Co_{0.1}Fe_{0.8}Cu_{0.1}O_{3-\delta}$ are larger than that of $La_{0.6}Sr_{0.4}Co_{0.2}Fe_{0.8}O_{3-\delta}$, suggesting that the doping of Cu^{2+} increased the Jahn–Teller distortion of the MO_6 octahedron and led to different transport properties [18].

The calcined and milled $La_{0.6}Sr_{0.4}Co_{0.2}Fe_{0.8}O_{3-\delta}$, $La_{0.6}Sr_{0.4}Co_{0.2}Fe_{0.7}Cu_{0.1}O_{3-\delta}$, and $La_{0.6}Sr_{0.4}Co_{0.1}Fe_{0.8}Cu_{0.1}O_{3-\delta}$ powders showed respectively an average particle size of 2.70, 2.86, and 2.96 μm. Fig. 2 presents the SEM micrographs of the $La_{0.6}Sr_{0.4}Co_{0.2}Fe_{0.8}O_{3-\delta}$ discs sintered at 1300 °C and 1100 °C, and the $La_{0.6}Sr_{0.4}Co_{0.2}Fe_{0.7}Cu_{0.1}O_{3-\delta}$ and the $La_{0.6}Sr_{0.4}Co_{0.1}Fe_{0.8}Cu_{0.1}O_{3-\delta}$ discs sintered at 1100 °C. Pure $La_{0.6}Sr_{0.4}Co_{0.2}Fe_{0.8}O_{3-\delta}$ reported a theoretical density of 98.95% (i.e., a sintered density of $6.30\,g\,cm^{-3}$) and an average grain size of 2.47 μm when sintered at 1300 °C for 2 h [Fig. 2(a)]. Since a $La_{0.6}Sr_{0.4}Co_{0.2}Fe_{0.8}O_{3-\delta}$ cathode is typically screen-printed on the electrolyte–anode substrates and post-fired at 1000–1100 °C, the sintering of LSCF was also performed at 1100 °C, and a theoretical density of 61.07% (i.e., a sintered density of $3.89\,g\,cm^{-3}$) and an average grain size of 0.39 μm were obtained, as shown in Fig. 2(b). Only neck growth among gains was observed while the densification process was absent after the firing process. For the Cu^{2+} doped $La_{0.6}Sr_{0.4}Co_{0.2}Fe_{0.8}O_{3-\delta}$ discs, the $La_{0.6}Sr_{0.4}Co_{0.2}Fe_{0.7}Cu_{0.1}O_{3-\delta}$ and the $La_{0.6}Sr_{0.4}Co_{0.1}Fe_{0.8}Cu_{0.1}O_{3-\delta}$ discs sintered at 1100 °C reached a theoretical density respectively of 90.00% and 86.80% (i.e., sintered densities of 5.73 and $5.53\,g\,cm^{-3}$, respectively), and the average grain sizes read 0.60 μm and 0.67 μm. It is apparent that densification was significantly enhanced by the Cu^{2+} ion substitution, a result consistent with the finding reported in the literature [16].

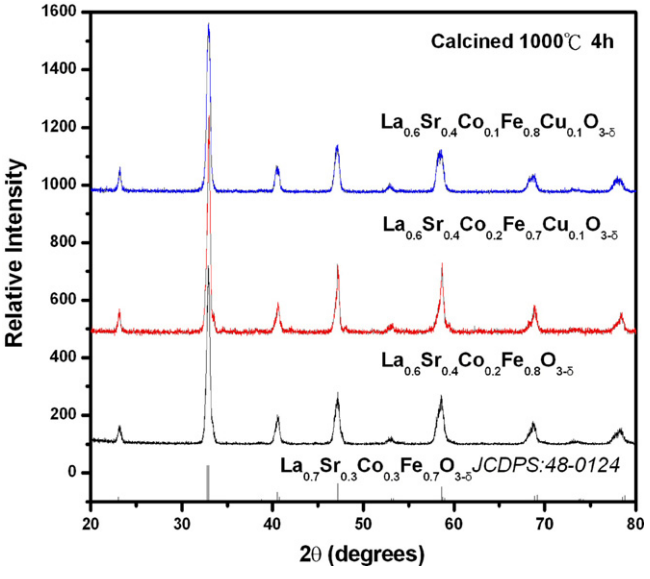

Fig. 1. XRD patterns of $La_{0.6}Sr_{0.4}Co_{0.2}Fe_{0.8}O_{3-\delta}$, $La_{0.6}Sr_{0.4}Co_{0.2}Fe_{0.7}Cu_{0.1}O_{3-\delta}$, and $La_{0.6}Sr_{0.4}Co_{0.1}Fe_{0.8}Cu_{0.1}O_{3-\delta}$ powders calcined at 1000 °C for 4 h.

The electrical conductivities, measured at ambient pressure in air, as a function of temperature for the $La_{0.6}Sr_{0.4}Co_{0.2}Fe_{0.8}O_{3-\delta}$ discs sintered at 1300 °C and 1100 °C, and for the $La_{0.6}Sr_{0.4}Co_{0.2}Fe_{0.7}Cu_{0.1}O_{3-\delta}$, and the $La_{0.6}Sr_{0.4}Co_{0.1}Fe_{0.8}Cu_{0.1}O_{3-\delta}$ discs sintered at 1100 °C were shown in Fig. 3. The conductivity of the perovskite cathodes increased with the temperature and reached its peak approximately between 300 °C and 600 °C, but started to drop with further rise in the temperature. The peak was reached probably due to the temperatures at which the oxygen exchange of the materials started to create an increasing number of vacancies to compete with hole carriers [19]. This was to be expected since Sr substitution is compensated by formation of oxygen vacancies and the tetravalent Co ad Fe in the perovskite lattices, according to $2[V_O^{\bullet\bullet}] + [Co_{Co}^{\bullet}] + [Fe_{Fe}^{\bullet}] = [Sr'_{La}]$ [20,21]. At lower temperatures ($T < 300$ °K), the conductivity shows a thermally activated behavior and increases with the temperature due to the increasing mobility of the electronic charge carriers, $Fe_{Fe}^{\bullet}$ and $Co_{Co}^{\bullet}$, which represent the holes localized on B sites. At higher temperatures, on the other hand, the electronic conductivity is reduced by the decrease in the number of p-type charge carriers due to the progressive formation of oxygen vacancies at the expense of $Fe_{Fe}^{\bullet}$ and $Co_{Co}^{\bullet}$ [10,22]. In agreement with the results reported in the literature [23], the sintered discs exhibited mixed ionic–electronic properties at temperatures beyond the peak, helping enhance the contribution of the bulk pathway to oxygen reduction. The discs, however, displayed mainly electronic properties and surface pathway at temperatures below the peak. Comparing the electrical conductivities of the $La_{0.6}Sr_{0.4}Co_{0.2}Fe_{0.8}O_{3-\delta}$, $La_{0.6}Sr_{0.4}Co_{0.2}Fe_{0.7}Cu_{0.1}O_{3-\delta}$, and $La_{0.6}Sr_{0.4}Co_{0.1}Fe_{0.8}Cu_{0.1}O_{3-\delta}$ discs sintered at 1100 °C as shown in Fig. 3, the study found the $La_{0.6}Sr_{0.4}Co_{0.2}Fe_{0.7}Cu_{0.1}O_{3-\delta}$ disc reporting a highest conductivity of $438\,S\,cm^{-1}$ at 400 °C, followed subsequently by the $La_{0.6}Sr_{0.4}Co_{0.1}Fe_{0.8}Cu_{0.1}O_{3-\delta}$ disc ($340\,S\,cm^{-1}$ at 400 °C) and the $La_{0.6}Sr_{0.4}Co_{0.2}Fe_{0.8}O_{3-\delta}$ disc ($81\,S\,cm^{-1}$ at 400 °C). The differences in the electrical conductivity may be caused by two major factors. First, the density of the $La_{0.6}Sr_{0.4}Co_{0.2}Fe_{0.8}O_{3-\delta}$ disc was much lower than those of its $La_{0.6}Sr_{0.4}Co_{0.2}Fe_{0.7}Cu_{0.1}O_{3-\delta}$ and $La_{0.6}Sr_{0.4}Co_{0.1}Fe_{0.8}Cu_{0.1}O_{3-\delta}$ counterparts when sintered at 1100 °C. The $La_{0.6}Sr_{0.4}Co_{0.2}Fe_{0.8}O_{3-\delta}$ disc sintered at 1300 °C was observed to result in a much higher electrical conductivity ($422\,S\,cm^{-1}$ at 600 °C), a finding in accord with that observed in the literature [24,25]. Another reason may lie in the Cu^{2+} substitution over the B-site ions, which generates a metallic conduction behavior [13]. The plots in Fig. 3(b) were nearly linear below the

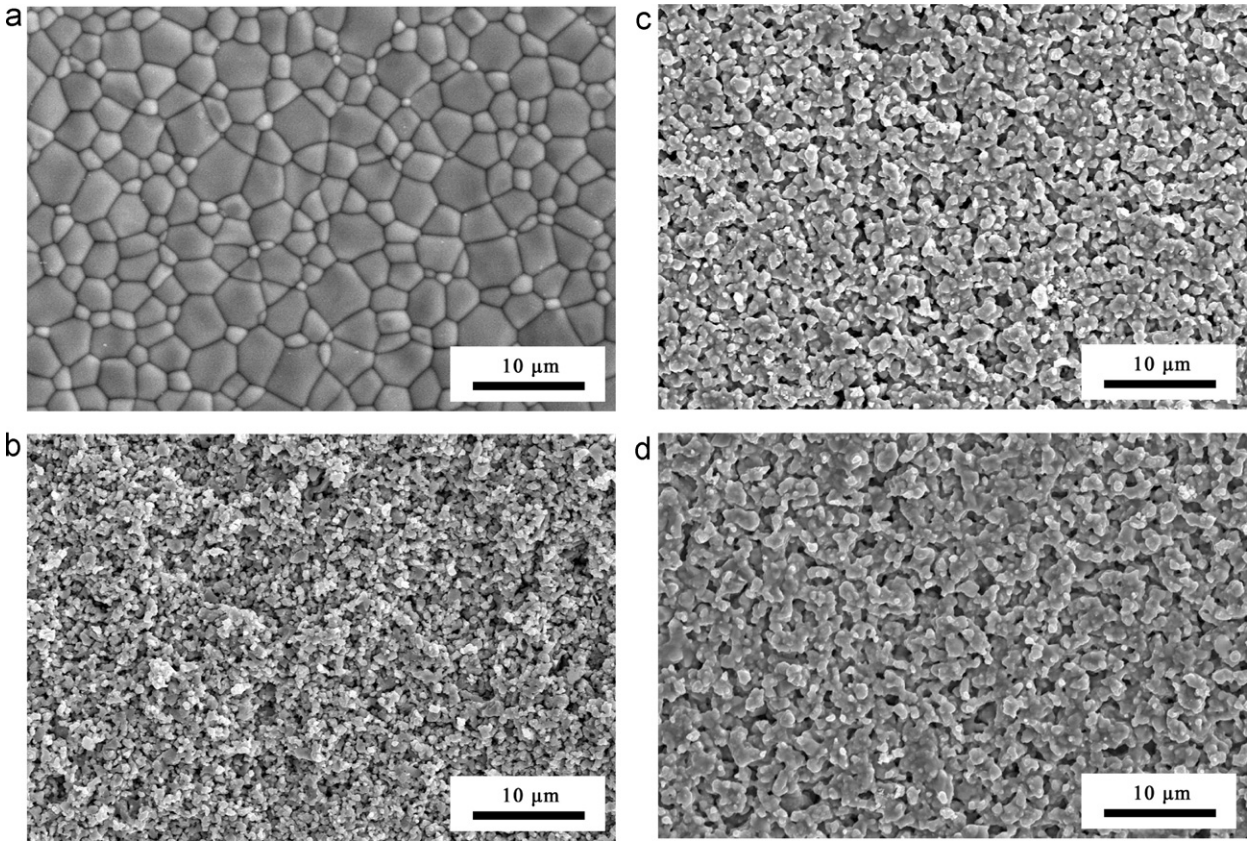

Fig. 2. Surface SEM micrographs of $La_{0.6}Sr_{0.4}Co_{0.2}Fe_{0.8}O_{3-\delta}$ discs sintered at (a) 1300 °C and (b) 1100 °C, and (c) $La_{0.6}Sr_{0.4}Co_{0.2}Fe_{0.7}Cu_{0.1}O_{3-\delta}$ and (d) $La_{0.6}Sr_{0.4}Co_{0.1}Fe_{0.8}Cu_{0.1}O_{3-\delta}$ discs sintered at 1100 °C.

temperature range at which the electrical conductivity reached its peak; this may suggest that the small polar on hopping is the predominant mechanism. The temperature dependence of the electrical conductivity was found to follow the relationship for the adiabatic small polar on hopping mechanism, which can be expressed as [21]:

$$\sigma = \left(\frac{A}{kT}\right) \exp\left(\frac{-E_a}{kT}\right),$$

In which A is a material constant containing the carrier concentration term; E_a is the activation energy for the hopping conduction; k is the Boltzmann constant. At higher temperatures, the plots indicate a substantial negative deviation from linearity due to the significant increase in oxygen vacancies [24,25].

The dilatometric curves of the $La_{0.6}Sr_{0.4}Co_{0.2}Fe_{0.8}O_{3-\delta}$, $La_{0.6}Sr_{0.4}Co_{0.2}Fe_{0.7}Cu_{0.1}O_{3-\delta}$, and $La_{0.6}Sr_{0.4}Co_{0.1}Fe_{0.8}Cu_{0.1}O_{3-\delta}$ discs are shown in Fig. 4. Calculated by fitting the dilatometric curves from 25 °C to 800 °C, the CTEs of the $La_{0.6}Sr_{0.4}Co_{0.2}Fe_{0.8}O_{3-\delta}$, $La_{0.6}Sr_{0.4}Co_{0.2}Fe_{0.7}Cu_{0.1}O_{3-\delta}$, and $La_{0.6}Sr_{0.4}Co_{0.1}Fe_{0.8}Cu_{0.1}O_{3-\delta}$ discs read, respectively $15.9 \times 10^{-6}\,K^{-1}$, $17.6 \times 10^{-6}\,K^{-1}$, and $12.2 \times 10^{-6}\,K^{-1}$ (Table 1). It is clear that substituting Cu^{2+} for Fe^{3+} led to a higher CTE while replacing Co^{3+} with Cu^{2+} resulted in a lower CTE, which is correlated to the bond length between metal ions and oxygen ions [26,27]. The CTE values are equal to or larger than that of the commonly used $Sm_{0.2}Ce_{0.8}O_{2-\delta}$ cathode (SDC: $12.6 \times 10^{-6}\,K^{-1}$) [28,29]. A composite cathode made of cathode and electrolyte materials is generally employed to minimize the CTE mismatch at the electrolyte/cathode interface [30]. The change in the slope of the dilatometric curves at approximately 330 °C, which resulted in an inflection point, was attributed to the beginning oxygen exchange of the materials [21,24,31]. A repulsion force arose between the mutually exposed cations when oxygen ions were extracted from the lattice, thus causing the lattice expansion. An additional chemical expansion took place due to the reduction of the Fe and Co ions from higher to lower valences (ex. Fe^{4+} ions were reduced to the larger Fe^{3+} ions), occurring in conjunction with the creation of oxygen vacancies (increasing oxygen non-stoichiometry) to retain the electrical neutrality at high temperatures [16,19]. This appears to be in agreement with the change in conductivity with the temperature as shown in Fig. 4.

Fig. 5 presents the cross-section SEM micrographs of the single cells with the $La_{0.6}Sr_{0.4}Co_{0.2}Fe_{0.8}O_{3-\delta}$, $La_{0.6}Sr_{0.4}Co_{0.2}Fe_{0.7}Cu_{0.1}O_{3-\delta}$, and $La_{0.6}Sr_{0.4}Co_{0.1}Fe_{0.8}Cu_{0.1}O_{3-\delta}$

Table 2
Ohmic and polarization resistances, open circuit voltages, and maximum power densities of the single cells with various cathodes measured at 650 °C and 550 °C.

Cathode materials for single cells	Maximum electrical conductivity (S cm^{-1})	R_0 (Ω-cm^2)		R_P (Ω-cm^2)		OCV (V)		MPD (Wcm^{-2})	
		650 °C	550 °C	650 °C	550 °C	650 °C	550 °C	650 °C	550 °C
$La_{0.6}Sr_{0.4}Co_{0.2}Fe_{0.8}O_{3-\delta}$	81 (400 °C)	0.045	0.120	0.105	0.212	0.74	0.75	1.03	0.46
$La_{0.6}Sr_{0.4}Co_{0.2}Fe_{0.7}Cu_{0.1}O_{3-\delta}$	438 (400 °C)	0.046	0.117	0.088	0.198	0.78	0.85	1.09	0.49
$La_{0.6}Sr_{0.4}Co_{0.1}Fe_{0.8}Cu_{0.1}O_{3-\delta}$	340 (350 °C)	0.051	0.122	0.079	0.200	0.80	0.85	1.17	0.49

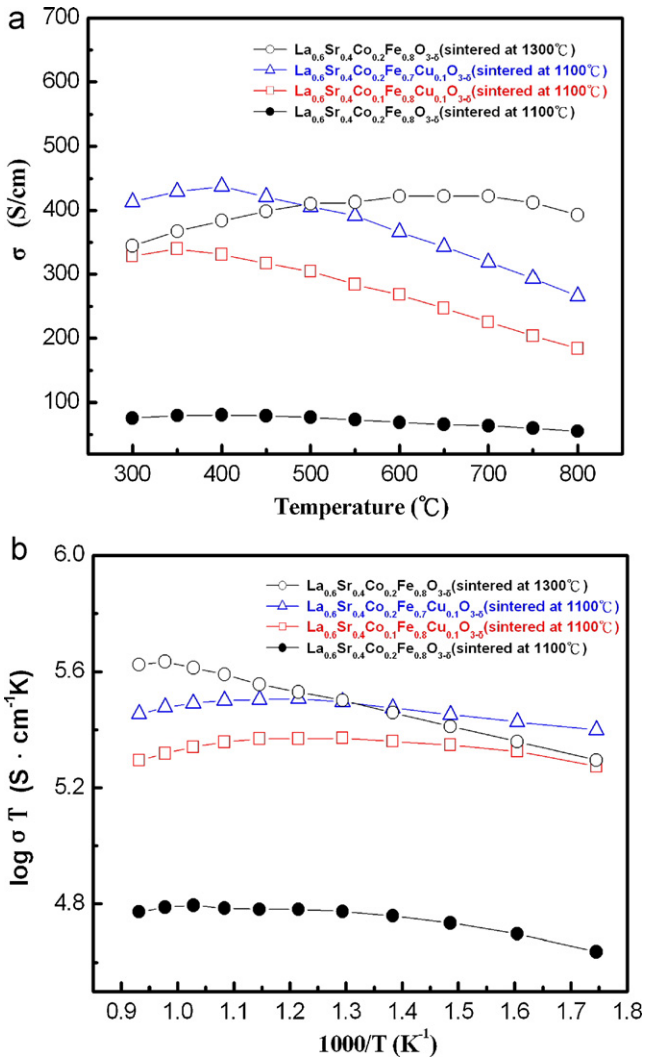

Fig. 3. (a) Electrical conductivities (σ) as a function of temperature and (b) $\log \sigma T$ versus 1000/T, measured at ambient pressure in air, for $La_{0.6}Sr_{0.4}Co_{0.2}Fe_{0.8}O_{3-\delta}$ discs sintered at 1300 °C and 1100 °C, and for $La_{0.6}Sr_{0.4}Co_{0.2}Fe_{0.7}Cu_{0.1}O_{3-\delta}$ and $La_{0.6}Sr_{0.4}Co_{0.1}Fe_{0.8}Cu_{0.1}O_{3-\delta}$ discs sintered at 1100 °C.

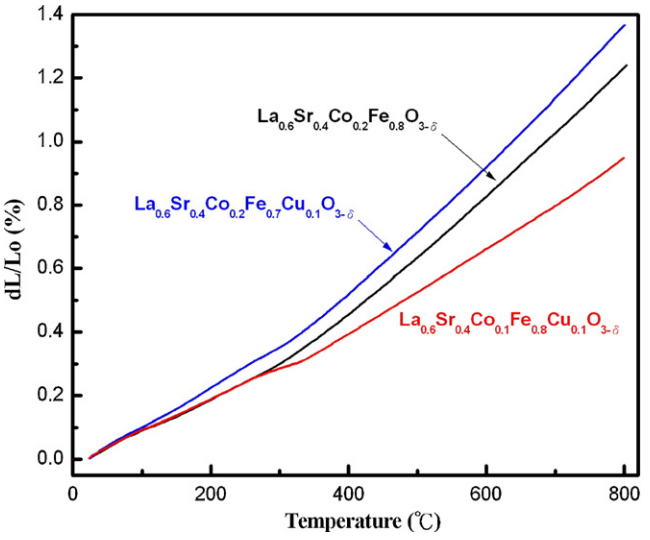

Fig. 4. Dilatometric curves of $La_{0.6}Sr_{0.4}Co_{0.2}Fe_{0.8}O_{3-\delta}$, $La_{0.6}Sr_{0.4}Co_{0.2}Fe_{0.7}Cu_{0.1}O_{3-\delta}$, and $La_{0.6}Sr_{0.4}Co_{0.1}Fe_{0.8}Cu_{0.1}O_{3-\delta}$ discs.

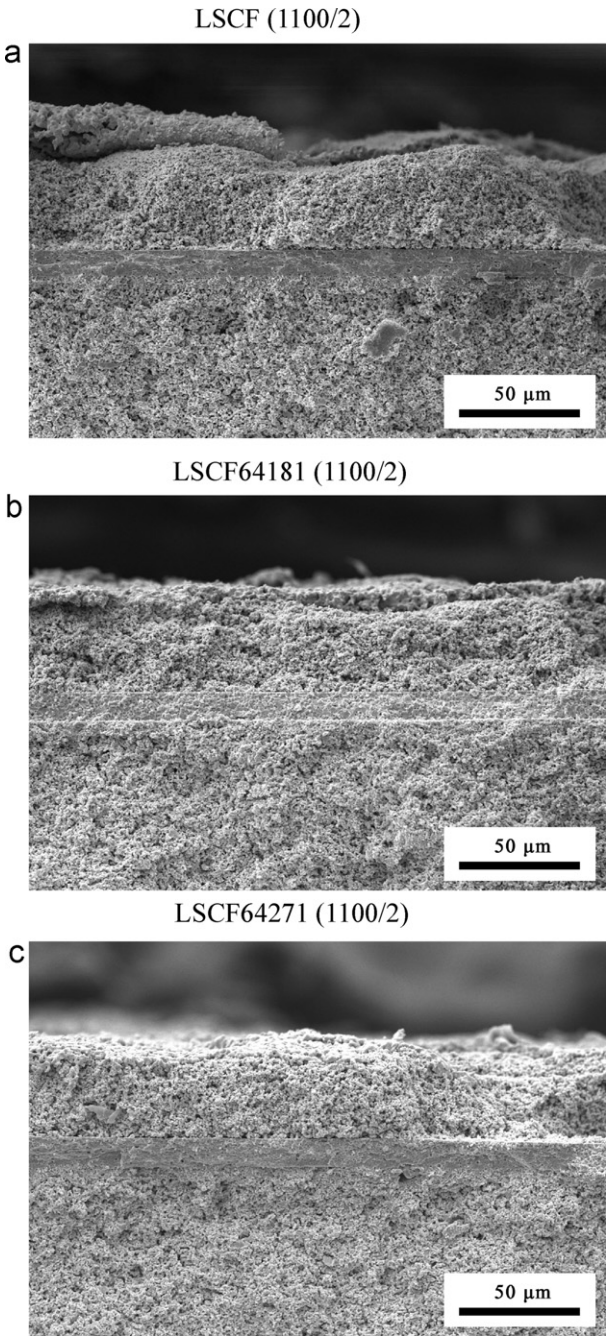

Fig. 5. Cross-section SEM micrographs of the single cells prepared in this study with (a) $La_{0.6}Sr_{0.4}Co_{0.2}Fe_{0.8}O_{3-\delta}$, (b) $La_{0.6}Sr_{0.4}Co_{0.1}Fe_{0.8}Cu_{0.1}O_{3-\delta}$, and (c) $La_{0.6}Sr_{0.4}Co_{0.2}Fe_{0.7}Cu_{0.1}O_{3-\delta}$ cathodes after electrochemical measurements.

cathodes prepared in this study after electrochemical measurements. It can be seen that the interfaces among the anode, electrolyte, and cathode layers for all cells show no sign of crack, delamination, or discontinuity. The SDC electrolyte with a thickness of nearly 13 μm is dense and crack-free with some scattering closed pores. The anode electrode, reporting a total thickness of approximately 0.5 mm, is composed of three layers, including a NiO current collector layer (thickness ≈20 μm) plus a 60 wt% NiO/40 wt% SDC (thicknesses ≈460 μm) and a 50 wt% NiO/50 wt% SDC (thickness ≈6 μm) functional composite layers. XRD analysis verified that the NiO at the anode was completely reduced to Ni after the electrochemical test. Both the anode and cathode layers were marked with the presence of porous

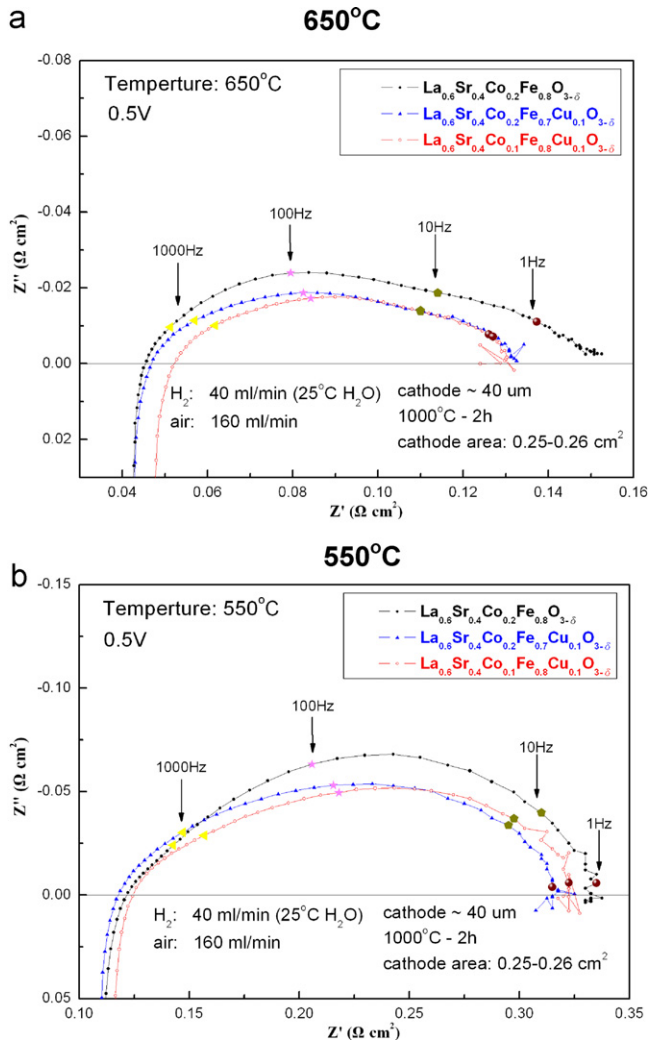

Fig. 6. Nyquist plots of electrochemical impedance spectra of the single cells containing $La_{0.6}Sr_{0.4}Co_{0.2}Fe_{0.8}O_{3-\delta}$, $La_{0.6}Sr_{0.4}Co_{0.2}Fe_{0.7}Cu_{0.1}O_{3-\delta}$, and $La_{0.6}Sr_{0.4}Co_{0.1}Fe_{0.8}Cu_{0.1}O_{3-\delta}$ cathodes measured at (a) 650 °C and (b) 550 °C.

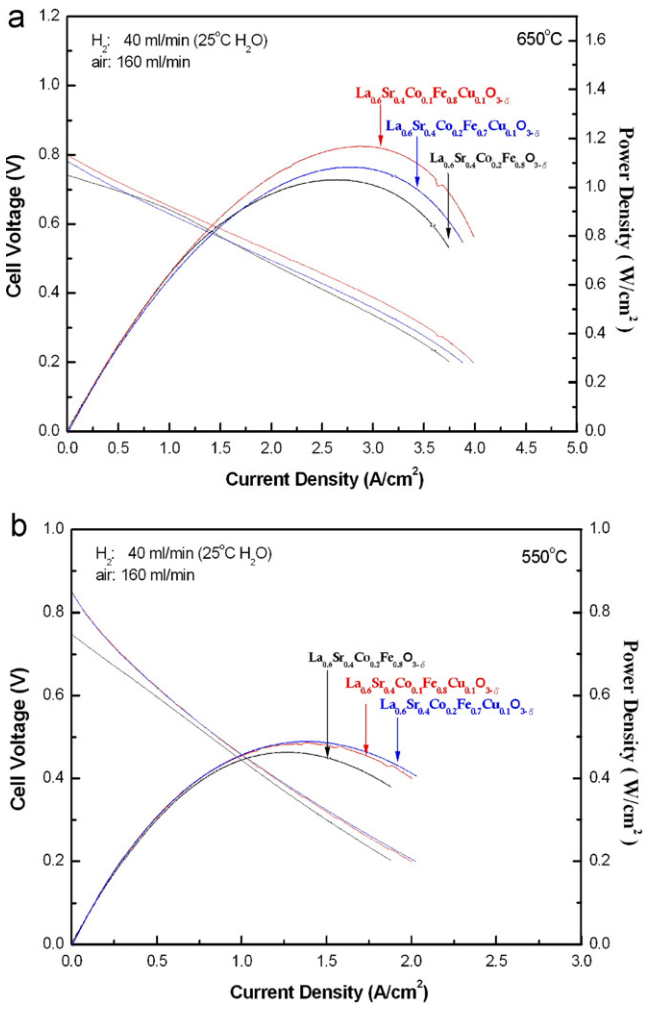

Fig. 7. *I–V* curves and the corresponding power densities of the anode supported single cells with various cathodes measured at (a) 650 °C and (b) 550 °C.

microstructures. The porosity contents of the $La_{0.6}Sr_{0.4}Co_{0.2}Fe_{0.8}O_{3-\delta}$, $La_{0.6}Sr_{0.4}Co_{0.2}Fe_{0.7}Cu_{0.1}O_{3-\delta}$, and $La_{0.6}Sr_{0.4}Co_{0.1}Fe_{0.8}Cu_{0.1}O_{3-\delta}$ cathode layers, measured by mercury porosimetry, read 60.3%, 46.3% and 45.9%, respectively, though their initial powder sizes were highly similar and firing conditions identical. The Cu^{2+} doped cathodes demonstrated better densification and thus lower porosity contents.

Fig. 6(a) and (b) shows the Nyquist plots of the electrochemical impedance spectra of the single cells with the $La_{0.6}Sr_{0.4}Co_{0.2}Fe_{0.8}O_{3-\delta}$, $La_{0.6}Sr_{0.4}Co_{0.2}Fe_{0.7}Cu_{0.1}O_{3-\delta}$, and $La_{0.6}Sr_{0.4}Co_{0.1}Fe_{0.8}Cu_{0.1}O_{3-\delta}$ cathodes measured at 650 °C and 550 °C, indicating that the inductive process caused by the measurement setup became noticeable at the high frequency of the spectra. The highest frequency intercept of the impedance spectra gives the total ohmic resistance of the cell (R_0), including the resistive contributions of the electrolyte, the two electrodes, the current collectors, and the lead wires, as reported in the literature [32–34]. The lowest frequency intercept corresponds to the overall resistance of the cell, and the distance between the two intercepts gives the total interfacial polarization resistance (R_P) [9]. The polarization loss resulting from the anode side was small enough to be disregarded as compared to its counterpart from the cathode side, as observed by Huang et al. [35], Xia and Liu [36], and Fu et al. [37]. In addition, since the anode/electrolyte substrates in all of the single cells were fabricated using the exactly same design and processing method in this study, the distinctions in R_P value of the single cells shown in the impedance spectra should be entirely accounted for by the differences in cathodes. The R_0 and R_P values of the single cells at 650 °C and 550 °C are presented in Table 2. At the measurement temperature of 650 °C, though the single cell with $La_{0.6}Sr_{0.4}Co_{0.1}Fe_{0.8}Cu_{0.1}O_{3-(}$ showed a slightly higher R_0 value, all three single cells had similar R_0 values (≈0.05 Ω-cm^2), which appeared to be lower than those reported in the literature [28,38]. At 550 °C, the ohmic resistance of these single cells increased from ≈0.05 Ω-cm^2 to ≈0.12 Ω-cm^2, clearly indicating that the increase in R_0 was caused by the low conductivity of the SDC electrolyte. As shown in Table 2, it is evident that the R_P value increased significantly as the temperature decreased. As illustrated in Fig. 6(b), the R_P values for all single cells at 550 °C were more than twice greater than those at 650 °C. The polarization resistances of the single cells with the $La_{0.6}Sr_{0.4}Co_{0.2}Fe_{0.7}Cu_{0.1}O_{3-\delta}$ and $La_{0.6}Sr_{0.4}Co_{0.1}Fe_{0.8}Cu_{0.1}O_{3-\delta}$ cathodes showed no significant difference and were slightly lower than that of the single cell with the $La_{0.6}Sr_{0.4}Co_{0.2}Fe_{0.8}O_{3-\delta}$ cathode. The R_P values of the single cells, lower than most of the results for the cells with LSCF cathodes shown in the literature [30,39,40], are expected to experience further decline if ≈40 wt% SDC electrolyte was added to form a composite cathode [40,41].

The cell performances for the single cells with various cathodes at 650 °C and 550 °C are shown in Fig. 7(a) and (b). The open

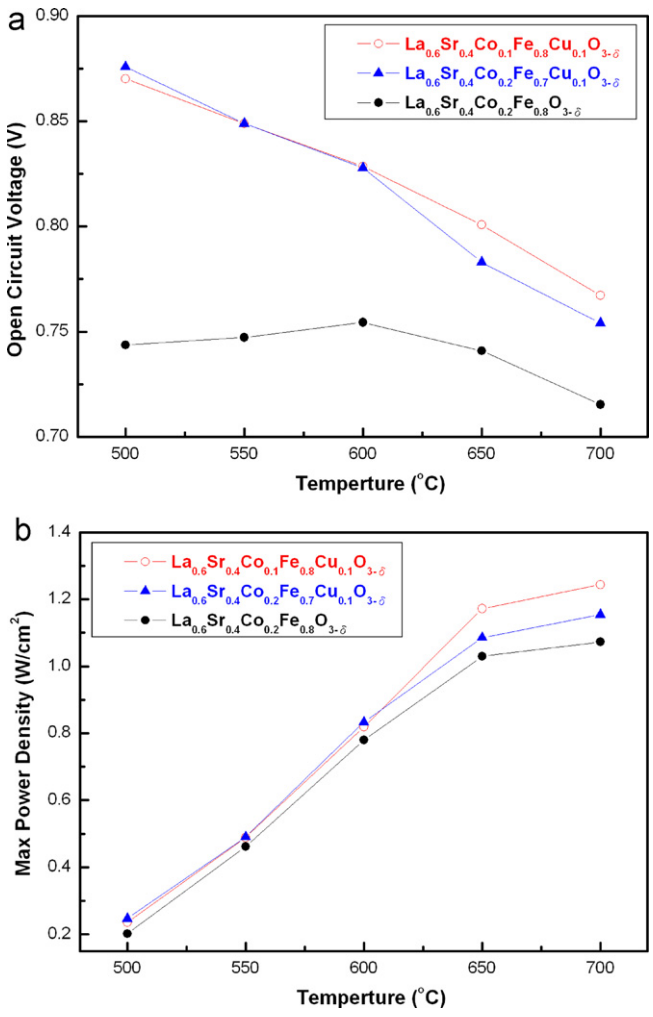

Fig. 8. (a) Open circuit voltages and (b) maximum power densities of the single cells with various cathodes measured at various temperatures.

circuit voltages (OCV) and maximum power densities (MPD) of the single cells operating at various temperatures are plotted in Fig. 8(a) and (b) and part of the results are listed in Table 2. The OCV of the single cells declined with the increase in temperature, dropping from 0.75 V at 500 °C to 0.72 V at 700 °C for the single cell with the $La_{0.6}Sr_{0.4}Co_{0.2}Fe_{0.8}O_{3-\delta}$ cathode, from 0.87 V to 0.77 V for the one with the $La_{0.6}Sr_{0.4}Co_{0.1}Fe_{0.8}Cu_{0.1}O_{3-\delta}$ cathode, and from 0.88 V to 0.75 V for the one with the $La_{0.6}Sr_{0.4}Co_{0.2}Fe_{0.7}Cu_{0.1}O_{3-\delta}$ cathode. The OCV values are lower than the expected theoretical values at higher temperatures mainly because of the electrolyte thickness effect occurred in the SDC electrolyte having mixed ionic and electronic conduction [5,42,43], particularly at temperatures higher than 600 °C. Two attributes responsible for the decrease in the OCV value of the cells with reduced film thickness were reported in the literature, including the increase in the oxygen permeation flux (as proposed by Duncan el al. [42]) and the rise in electron flux (as suggested by Ding et al. [43]) as the SDC electrolyte gets thinner. With decreasing temperature, OCV value gradually rose as the electronic conduction degraded at lower temperatures. As indicated in Fig. 8(a), the single cell with the $La_{0.6}Sr_{0.4}Co_{0.2}Fe_{0.8}O_{3-\delta}$ cathode has the lowest OCV while the single cells with the $La_{0.6}Sr_{0.4}Co_{0.2}Fe_{0.7}Cu_{0.1}O_{3-\delta}$, and $La_{0.6}Sr_{0.4}Co_{0.1}Fe_{0.8}Cu_{0.1}O_{3-\delta}$ cathodes have a similar OCV at temperatures ranging from 500 °C to 600 °C, and the OCVs at 650 °C and 700 °C of the single cell with the $La_{0.6}Sr_{0.4}Co_{0.1}Fe_{0.8}Cu_{0.1}O_{3-\delta}$ cathode were slightly higher than those of the single cell with the $La_{0.6}Sr_{0.4}Co_{0.2}Fe_{0.7}Cu_{0.1}O_{3-\delta}$ cathode. Fig. 8(b) indicates that MPD declined with decreasing operating temperature due to the increase in the R_0 and R_P values of the single cells as shown in Fig. 6 and Table 2. Of the three single cells, the one with the $La_{0.6}Sr_{0.4}Co_{0.1}Fe_{0.8}Cu_{0.1}O_{3-\delta}$ cathode was observed to report the highest MPD, and the cell with the $La_{0.6}Sr_{0.4}Co_{0.2}Fe_{0.8}O_{3-\delta}$ cathode the lowest at all temperatures measured. The maximum power densities of the single cell with the single-phase LSCF-based cathode (1.07 and 0.46 W cm^{-2} at 650 °C and 550 °C) are consistent with those reported in the literature [44–46], though their designs and preparation methods among the single cells are not exactly the same. The MPDs for the single cells with the $La_{0.6}Sr_{0.4}Co_{0.2}Fe_{0.8}O_{3-\delta}$, $La_{0.6}Sr_{0.4}Co_{0.2}Fe_{0.7}Cu_{0.1}O_{3-\delta}$, and $La_{0.6}Sr_{0.4}Co_{0.1}Fe_{0.8}Cu_{0.1}O_{3-\delta}$ cathodes were respectively 1.07, 1.15, and 1.24 W cm^{-2} at 650 °C. It is evident that the doping of Cu^{2+} ions in LSCF is beneficial to the electrochemical performance of the electrode.

4. Conclusions

In this study, the electrical conductivities of the $La_{0.6}Sr_{0.4}Co_{0.2}Fe_{0.7}Cu_{0.1}O_{3-\delta}$ and $La_{0.6}Sr_{0.4}Co_{0.1}Fe_{0.8}Cu_{0.1}O_{3-\delta}$ discs were higher than that of the $La_{0.6}Sr_{0.4}Co_{0.2}Fe_{0.8}O_{3-\delta}$ disc sintered at 1100 °C. The coefficients of thermal expansion of the $La_{0.6}Sr_{0.4}Co_{0.2}Fe_{0.8}O_{3-\delta}$, $La_{0.6}Sr_{0.4}Co_{0.2}Fe_{0.7}Cu_{0.1}O_{3-\delta}$, and $La_{0.6}Sr_{0.4}Co_{0.1}Fe_{0.8}Cu_{0.1}O_{3-\delta}$ discs read respectively 15.9×10^{-6}, 17.6×10^{-6}, and 12.2×10^{-6} K^{-1}. SOFCs using NiO–SDC, SDC, and LSCF–SDC, respectively, as anode, electrolyte, and cathode were built and characterized. The cells were similar in ohmic resistance while the polarization resistances of the cells with the $La_{0.6}Sr_{0.4}Co_{0.2}Fe_{0.7}Cu_{0.1}O_{3-\delta}$ and $La_{0.6}Sr_{0.4}Co_{0.1}Fe_{0.8}Cu_{0.1}O_{3-\delta}$ cathodes were slightly lower than that of the cell with the LSCF cathode, indicating that the Cu^{2+}-doped LSCF cathode exhibited greater electrochemical catalytic activity for oxygen reduction. Of the three single cells, the one with $La_{0.6}Sr_{0.4}Co_{0.1}Fe_{0.8}Cu_{0.1}O_{3-\delta}$ cathode reported the highest MPD. It is evident that the doping of Cu^{2+} ions in LSCF is capable of enhancing the electrochemical performance of the cells.

References

[1] M.D. Mata, X. Liub, Z. Zhu, B. Zhu, Int. J. Hydrogen Energy 32 (2007) 796–801.
[2] T.L. Wen, D. Wang, M. Chen, H. Tu, Z. Lu, Z.R. Zhang, H. Nie, Solid State Ionics 148 (2002) 513–519.
[3] E. Ivers-Tiffée, A. Weber, D. Herbstritt, J. Eur. Ceram. Soc. 21 (2001) 1805–1811.
[4] M. Zhang, M. Yang, Z. Hou, Y. Dong, M. Cheng, Electrochim. Acta 53 (2008) 4998–5006.
[5] J.W. Fergus, J. Power Sources 162 (2006) 30–40.
[6] S.B. Adler, Chem. Rev. 104 (2004) 4791–4843.
[7] J.M. Ralph, A.C. Schoeler, M. Krumpelt, J. Mater. Sci. 36 (2001) 1161–1172.
[8] J.M. Ralph, C. Rossignol, R. Kumar, J. Electrochem. Soc. 150 (2003) A1518–A1522.
[9] W.G. Guo, J. Liu, C. Jin, H. Gao, Y. Zhang, J. Alloys Compd. 473 (2009) 43–47.
[10] M. Prestat, J.F. Koenig, L.J. Gauckler, J. Electroceram. 18 (2007) 87–101.
[11] X. Ding, X. Kong, J. Jiang, C. Cui, L. Guo, Int. J. Hydrogen Energy 35 (2010) 1742–1748.
[12] S.F. Wang, Y.R. Wang, C.T. Yeh, Y.F. Hsu, S.D. Chyou, W.T. Lee, J. Power Sources 196 (2011) 977–987.
[13] H.C. Yu, K.Z. Fung, J. Power Sources 133 (2004) 162–168.
[14] K. Yasumoto, Y. Inagaki, M. Shiono, M. Dokiya, Solid State Ionics 148 (2002) 545–549.
[15] S.P. Simner, M.D. Anderson, J.W. Stevenson, J. Am. Ceram. Soc. 87 (2004) 1471–1476.
[16] U.F. Vogt, P. Holtappels, J. Sfeir, J. Richter, S. Duval, D. Wiedenmann, Fuel Cells 09 (2009) 899–906.
[17] Q. Pu, G. Xu, Z. Zhang, Z. Ding, Physics C 370 (2002) 163–168.
[18] S.P. Simner, M.D. Anderson, J. Bonnett, J. Stevenson, Solid State Ionics 175 (2004) 79–81.
[19] P. Ried, P. Holtappels, A. Wichser, A. Ulrich, T. Graule, J. Electrochem. Soc. 155 (2008) B1029–B1035.
[20] W. Sitte, E. Bucher, W. Preis, Solid State Ionics 154–155 (2002) 517–522.
[21] L.W. Tai, M.M. Nasrallah, H.U. Anderson, D.M. Sparlin, S.R. Sehlin, Solid State Ionics 76 (1995) 259–271.

[22] E. Bucher, W. Sitte, Solid State Ionics 173 (2004) 23–28.
[23] A. Esquirol, N.P. Brandon, J.A. Kilner, M. Mogensen, J. Electrochem. Soc. 151 (2004) A1847–A1855.
[24] L.W. Tai, M.M. Nasrallah, H.U. Anderson, D.M. Sparlin, S.R. Sehlin, Solid State Ionics 76 (1995) 273–283.
[25] D. Huang, X.U. Qing, Z. Feng, W. Chen, H. Liu, J. Zhou, J. Wuhan Univ. Technol. Mater. Sci. Ed. 23 (2008) 81–84.
[26] A.R. Ruffa, J. Mater. Sci. 15 (1980) 2258–2267.
[27] A.R. Ruffa, J. Mater. Sci. 15 (1980) 2268–2274.
[28] X. Ding, C. Cui, L. Guo, J. Alloys Compd. 481 (2008) 845–850.
[29] H.J. Hwang, J.W. Moon, S. Lee, E.A. Lee, J. Power Sources 145 (2005) 243–248.
[30] Y. Leng, S.H. Chan, Q. Liu, Int. J. Hydrogen Energy 33 (2008) 3808–3817.
[31] A. Fossdal, M. Menon, I. Waernhus, K. Wiik, M.A. Einarsrud, T. Grande, J. Am. Ceram. Soc. 87 (2004) 1952–1958.
[32] E.P. Murray, T. Tsai, S.A. Barnett, Solid State Ionics 110 (1998) 235–247.
[33] E.P. Murray, S.A. Barnett, Solid State Ionics 143 (2001) 265–273.
[34] Fuel Cell Handbook 7th edition, EG&G Technical Services, Inc., USDOE, pp. 7–18.
[35] Q.A. Huang, R. Hui, B. Wang, J. Zhang, Electrochim. Acta 52 (2007) 8144–8164.
[36] C. Xia, M. Liu, Adv. Mater. 14 (2002) 521–523.
[37] C. Fu, S.H. Chan, Q. Liu, X. Ge, G. Pasciak, Int. J. Hydrogen Energy 35 (2010) 301–307.
[38] X. Xu, C. Xia, G. Xiao, D. Peng, Solid State Ionics 176 (2005) 1513–1520.
[39] J. Zhang, Y. Ji, H. Gao, T. He, J. Liu, J. Alloys Compd. 395 (2005) 322–325.
[40] E.P. Murray, M.J. Sever, S.A. Barnett, Solid State Ionics 148 (2002) 27–34.
[41] M. Shah, J.D. Nicholas, S.A. Barnett, Electrochem. Commun. 11 (2009) 2–5.
[42] K.L. Duncan, K.T. Lee, E.D. Wachsman, J. Power Sources 196 (2011) 2445–2451.
[43] C. Ding, H. Lin, K. Sato, K. Amezawa, T. Kawada, J. Mizusaki, T. Hashida, J. Power Sources 195 (2010) 5487–5492.
[44] J.S. Ahn, H. Yoon, K.T. Lee, M.A. Camaratta, E.D. Wachsman, Fuel Cells 9 (2009) 643–649.
[45] Y. Xie, R. Neagu, C.S. Hsu, X. Zhang, C. Deces-Petit, W. Qu, R. Hui, S. Yick, M. Robertson, R. Maric, D. Ghosh, J. Fuell Cell Sci. Tech. 7 (2010) 021007.
[46] M. Chen, B.H. Kim, Q. Xu, B.G. Ahn, D.P. Huang, J. Membr. Sci. 360 (2010) 461–468.